AIP ADVANCES **1**, 042113 (2011)

Quantitative characterization of acid concentration and temperature dependent self-ordering conditions of anodic porous alumina

Chuan Cheng,[a] K. Y. Ng, and A. H. W. Ngan
Department of Mechanical Engineering, The University of Hong Kong, Pokfulam Road, Hong Kong, P. R. China

(Received 28 June 2011; accepted 26 September 2011; published online 12 October 2011)

Acid concentration and temperature dependent self-ordering conditions of anodic porous alumina formed by anodization of aluminum in oxalic acid are quantitatively characterized by a new technique involving the distribution of the angular orientation of the triangles formed by neighboring pore centers, in order to detect the self-ordering domains in each porous pattern. This technique is found to be more sensitive in quantifying ordering of the patterns than the radial distribution function and angle distribution function. Using this technique, the optimal acid concentration which can result in the best self-ordering of the porous alumina under a given temperature is established. The optimal acid concentration is found to be approximately linearly increasing with temperature. The oxide growth rate increases approximately exponentially with acid concentration and also with temperature. The results suggest that anodization conducted at relatively higher temperatures at the corresponding optimal acid concentrations can enable fast production of self-ordered anodic porous alumina for industrial applications. [doi:10.1063/1.3655416]

I. INTRODUCTION

Anodic porous alumina, which is fabricated by anodization of aluminum with pore sizes in the range of tens to hundreds of nanometers and arranged in a quasi periodic hexagonal pattern,[1–3] has been extensively studied for use as an excellent template material for fabricating nano-structured materials, such as nano-wire arrays,[4] nano-tubes,[5] nano-capacitors,[6] and photonic crystals.[7] In these applications, one usual requirement is that the arrangement of the pore-channels inside the porous alumina should be hexagonally self-ordered, and this means that the growth of the pore-channels during aluminum anodization should be a self-ordering process[1,2] with as infrequent splitting, merging or termination as possible.[8,9] Plenty of previous efforts have been made to find the anodization conditions which can result in self-ordering porous alumina patterns. Masuda and Fukuda found that mild anodization conducted in 0.3 M oxalic acid at 40 V at 0 °C can result in self-ordering patterns.[1] A two-step anodization method,[1,10] in which the second anodization step starts from the pre-textured patterns resulted from a first anodization step, can improve the self-ordering of the pore-channel growth. Similarly, suitable pre-textures for enhancing ordering pore-channel growth can also be deliberately made by nano-imprinting of the aluminum substrate,[11–14] although this method may not be as economical as just taking advantage of an intrinsic ability for the pore-channels to self-adjust towards ordering under an optimal anodization condition of electrolyte, voltage and temperature.[15] In previous efforts to establish the self-ordering conditions, for a given type of electrolyte, its concentration was usually restricted in a narrow region, e.g. 0.3 M for oxalic acid,[1,16] 0.3 M for sulfuric acid,[16] and 0.1 M for phosphoric acid,[17] and there has been rare

[a]Author to whom correspondence should be addressed. E-mail: chuan@hku.hk. Present address: Beckman Institute for Advanced Science and Technology, University of Illinois at Urbana-Champaign, IL 61801, USA

systematic investigation on the effects of acid concentration in a wide range, for example throughout the solubility limit of the acid solution at a given temperature, on the self-ordering of the porous pattern.

Another important requirement for the industrial-scale application of anodic porous alumina is that the anodic oxide growth rate should be fast. However, under traditional mild anodization conditions, in order to obtain the self-ordering pore arrangement, the anodization is usually conducted under low temperatures and voltages, so that the oxide growth rate is usually several micrometers per hour,[2,17] and this may be too slow for batch production. Hard anodization, conducted under low temperatures but high anodization voltages or current densities, provides an effective means to increase oxide growth rate while maintaining the self-ordering pore arrangment.[2,15,17,18] We think that besides hard anodization, by increasing the acid concentration as well as temperature under the common voltages (e.g. 40 V with oxalic acid) often used in mild anodization,[1] self-ordering pore-channel growth may also be achievable yet the oxide growth would be significantly accelerated. The aim of the present work is therefore to study the self-ordering quality of anodic porous alumina fabricated at 40 V in oxalic acid, of a wide concentration range spanning the solubility limit of oxalic acid in water, under different temperatures. To quantitatively characterize the ordering quality of the porous patterns, a new technique further developed from Hillebrand *et al*.[19] and Mátéfi-Tempfli *et al*.[20] is also presented in this paper, in which triangles formed by three neighboring pore centers are colored according to their angular orientation. The results computed by this technique are compared with the more usual representations of the radial distribution function[21] and angle distribution function.[19]

II. METHODS

A. Experimental methods

The anodization method used in this work is similar to that of Ng[22] and here, we just give a brief description. 99.99% pure aluminum foils were used for anodization, which were annealed under vacuum ($\sim 10^{-5}$ torr) at 500 °C for 24 h. The aluminum foils were then mechanically polished and electropolished in a mixed solution of $HClO_4$ and C_2H_5OH with composition 1 : 4 by volume. The anodization was conducted under a constant voltage of 40 V in oxalic acid of different concentration under 20 °C, 10 °C, and 2 °C. The aluminum foils were mounted on a copper plate serving as the anode, while the cathode is graphite. The anode and cathode were separated at a constant distance of ∼10 cm, and the area of aluminum exposed to the electrolyte was of 1 inch in diameter. During anodization the electrochemical cell was in a constant temperature environment achieved by an electronic feed-back controlled water bath. After anodization, in order to observe the pore arrangements at the pore bottom, oxide-metal interface region, the samples were put into a mixed solution of H_2CrO_4, H_3PO_4 and H_2O with composition 1.8 : 6 : 92.2 by weight at 60 °C, to selectively dissolve the anodic oxide away. Because of the scalloped shape of the oxide barrier layer at the pore bottom, each pore will leave behind a small dimple on the aluminum substrate, and so microscopic examination of the dimpled aluminum substrate after the selective dissolution of the alumina on top would directly reveal the arrangement of the pores at the end of the anodization. Scanning electron microscopy (SEM) examination was carried out in a Hitachi S-4800 field-emission microscope, and a LEO 1530 field-emission microscope. In the anodization experiments under 20 °C and 10 °C, two-step anoidzation was conducted, in which the second anodization step started from the pre-textured aluminum substrate after selectively removing the formed porous alumina in the first anodization step, and the first and second steps were carried out at the same anodization conditions. In the anodization under 2 °C, only one-step anodization was conducted, but actually for the long anodization time used, the pore arrangement has already reached a steady state corresponding to that anodization condition.

B. Pattern qualification methods

In order to quantitatively evaluate the ordering quality of different porous alumina patterns, the coordinates of the pore centers in each pattern were captured by the ImagJ software[23] as previously

used by Hillebrand *et al*..[19] Three analysis methods were used to quantify the pore ordering on the patterns as follows:

1. Radial distribution function (RDF)

The two-dimensional RDF is defined as

$$RDF = \frac{S_{pattern}}{2\pi r N}\frac{dn(r)}{dr}, \tag{1}$$

where $S_{pattern}$ is the pattern area, r is the distance between the centers of any two pores in the pattern, N is the total number of pore pairs, and $n(r)$ is the number of pore pairs in which the pores are separated by a distance $\leq r$. The RDF gives the probability density of finding a neighbor pore distanced r away from any given pore in the pattern.

2. Angle distribution function (ADF)

In a porous pattern, three nearest-neighboring pores form one triangle, and so the whole pattern can be represented as a mesh of triangles with the pore centers as the mesh nodes. In order to avoid unwanted side affects, the nearest neighbors of a given pore are found in a region around that pore center which is less than 1.8 times of the first RDF peak position, and each angle of a triangle should be in the range of 30° to 90° or else that triangle is not formed. Sometimes, in a disordered pattern, edges from two different triangles may intersect each other, and in this case, the triangle whose three edges have a smaller standard deviation (Dev_d) will be chosen. For a triangle, Dev_d is defined as[19,20]

$$Dev\_d = \frac{1}{\bar{d}}\sqrt{\frac{1}{3}\sum_{i=1}^{3}(d_i - \bar{d})^2} \tag{2}$$

where d_i ($i = 1, 2, 3$) are the edge lengths of that triangle, and $\bar{d}$ is the mean of d_i. The angles of all the formed triangles are statistically evaluated to give the angle distribution function (ADF), which represents the probability of finding a particular angle value in the pattern.[19]

3. Angular orientation distribution (AOD)

In the following analysis involving Figures 1 and 2, we will see that RDF and ADF are helpful when the differences in ordering qualities of the porous patterns are large; however, they are not sensitive enough to distinguish between patterns with close but different ordering qualities. A more sensitive method based on the orientation of the triangles formed in the ADF representation is proposed here. For any given triangle in the ADF representation described in Section II B 2 above, as shown in the examples below the color bar of Figure 3, its orientation θ with the SEM image horizontal boarder as the reference direction can be calculated as

$$\theta = \frac{1}{3}\left[\mathbf{atan}\left(\frac{y_1 - y_2}{x_1 - x_2}\right) + \mathbf{atan}\left(\frac{y_2 - y_3}{x_2 - x_3}\right) + \mathbf{atan}\left(\frac{y_3 - y_1}{x_3 - x_1}\right)\right]\frac{180^{\circ}}{\pi} \tag{3}$$

where (x_i, y_i), $i = 1, 2, 3$, are the coordinates of three vertices of the triangle. Most of the triangles in a mildly disordered pattern usually have θ calculated from equation (3) falling in the range [-30°, 30°], but if θ does exceed this range, it is reduced to within [-30°, 30°] by adding or subtracting 60°, because the mesh structure is a hexagonal arrangement of the triangles. The triangles are then colored according to their θ values with the wrapping scale shown at the top of Figure 3, in which -30° and 30° correspond to the same (red) color.

In order to distinguish grains in the pattern, which are ordering domains in which the triangles are similarly oriented, and then to calculate the average grain size, as is similar to Refs. 19 and 20, tolerance deviations of Tol_d and Tol_ϕ are introduced. For a given triangle, if its $Dev\_d < Tol\_d$

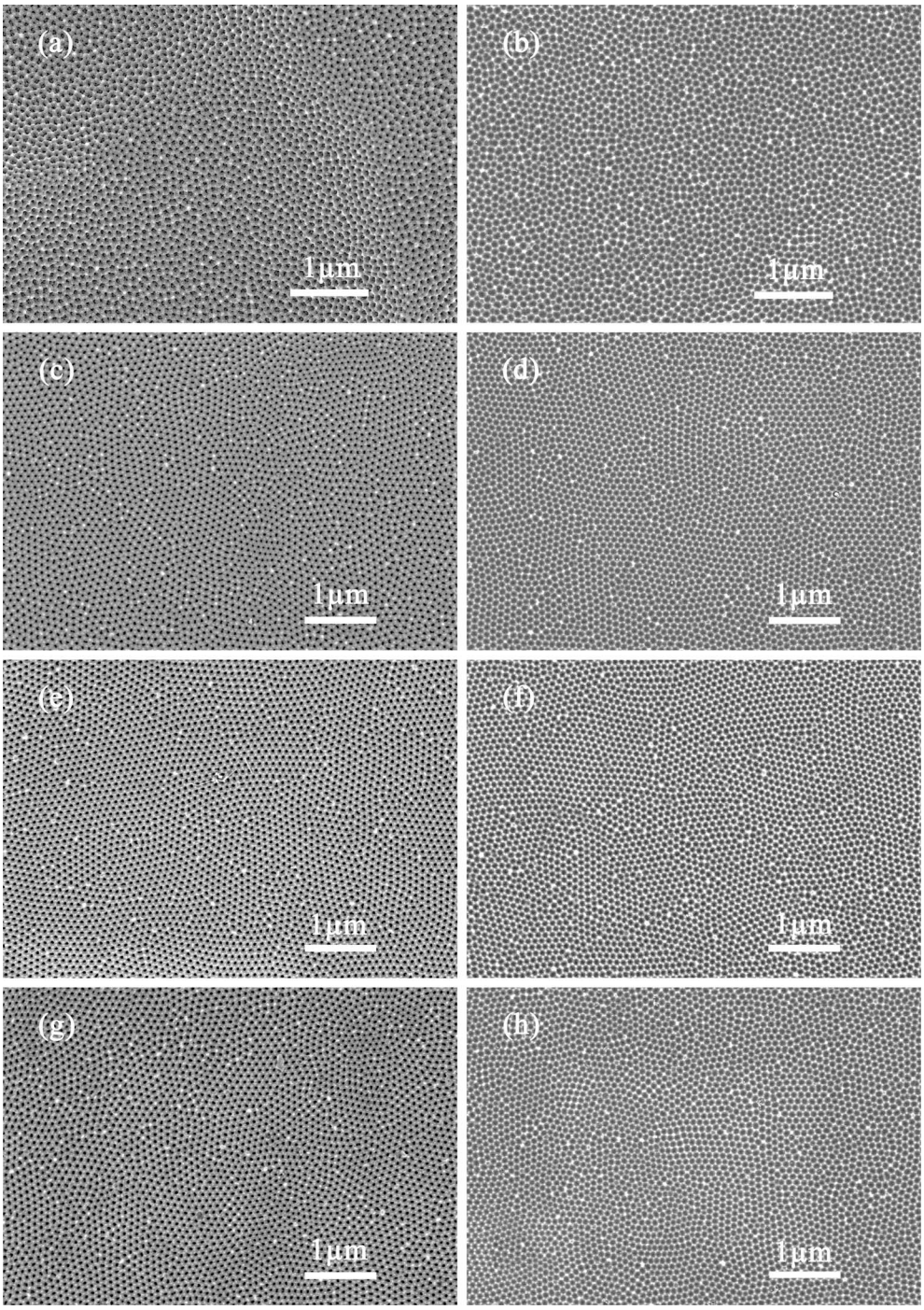

FIG. 1. SEM micrographs of (a, c, e, g) the top patterns of anodic porous alumina obtained by a second anodization step using Al substrates pre-textured in a first anodization step; (b, d, f, h) the bottom patterns of the aluminum substrate after selectively removing the anodic porous alumina on top. Two-step anodization was conducted in (a, b) 0.3 M; (c, d) 0.6 M; (e, f) 0.8 M; (g, h) 0.95 M oxalic acid at 40 V at 20 °C, with first step for 1 h and second step for 0.5 h.

and $Dev\_\phi < Tol\_\phi$, this triangle will be regarded as within the grains (ordering domains), where

$$Dev\_\phi = \frac{1}{\bar{\phi}}\sqrt{\frac{1}{3}\sum_{i=1}^{3}(\phi_i - \bar{\phi})^2} \tag{4}$$

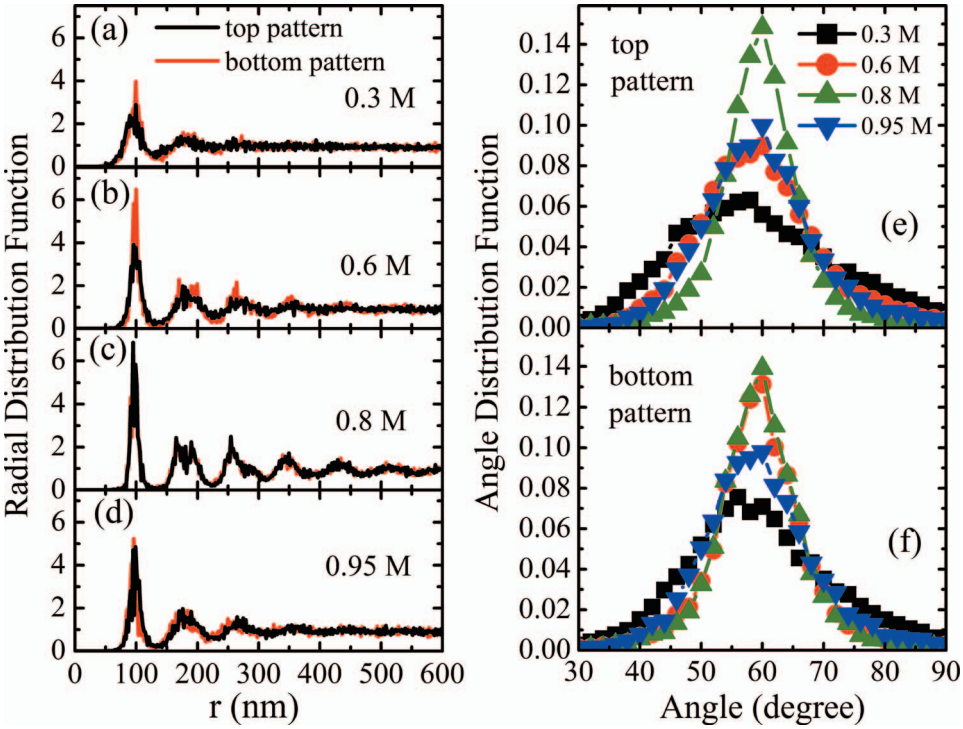

FIG. 2. (a-d) Radial distribution function for patterns shown in Figures 1(a)–1(h), respectively. (e, f) Angle distribution function for patterns shown in Figures 1(a), 1(c), 1(e), and 1(g) and 1(b), 1(d), 1(f), and 1(h), respectively.

is the standard deviation of the three angles ϕ_i ($i = 1, 2, 3$) in that given triangle, and $\bar{\phi}$ is the mean of ϕ_i. Because in real porous patterns, neighboring triangles within the same grain may not have exactly the same orientation θ, here we introduce a third tolerance parameter Tol_θ, which means that if the difference in orientation θ between two neighboring triangles $\Delta\theta < Tol\_\theta$, these two triangles are regarded as within the same grain (ordering domain). In the following, the use of the three tolerance conditions involving Tol_d, Tol_ϕ, and Tol_θ will be illustrated by examples.

III. RESULTS AND DISCUSSION

In Figures 1(a)–1(h), two-step anodization experiments were conducted in 0.3 M, 0.6 M, 0.8 M, and 0.95 M oxalic acid respectively, while other anodization conditions, namely, voltage of 40 V, temperature of 20 °C, and duration of 1 h for the first step and 0.5 h for the second step, were kept as the same. Figures 1(a), 1(c), 1(e), and 1(g) are SEM micrographs of the top views of the anodic porous alumina obtained by a second anodization step using Al substrates pre-textured in a first anodization step, and Figures 1(b), 1(d), 1(f), and 1(h) are SEM micrographs of the dimpled Al substrate after the selective dissolution of the oxide obtained in the second anodization step, revealing the ordering of the pore-channels at their bottom at the end of the second anodization step. From direct observation of these SEM images, a trend of the ordering tendency of the pore-channels with changing acid concentration is not obvious. For example, at a first glance, one may find that the ordering quality in Figure 1(a) is lower than that in Figure 1(c), but it is hard to distinguish the difference amongst Figures 1(c), 1(e), and 1(g) or Figures 1(d), 1(f), and 1(h). Thus, the quantitative pattern characterization methods introduced in Section II B were employed.

In Figure 2, the RDF and ADF are plotted for each pattern shown in Figure 1. By comparing the RDF in Figures 2(a)–2(d), on increasing acid concentration, ordering first increases from 0.3 M to 0.6 M, and then decreases from 0.8 M to 0.95 M, but the difference in ordering between 0.6 M and 0.8 M is not clear. In addition, the ordering difference between the top and bottom patterns for each anodization condition is small, except that at 0.6 M the first peak in the bottom pattern is stronger

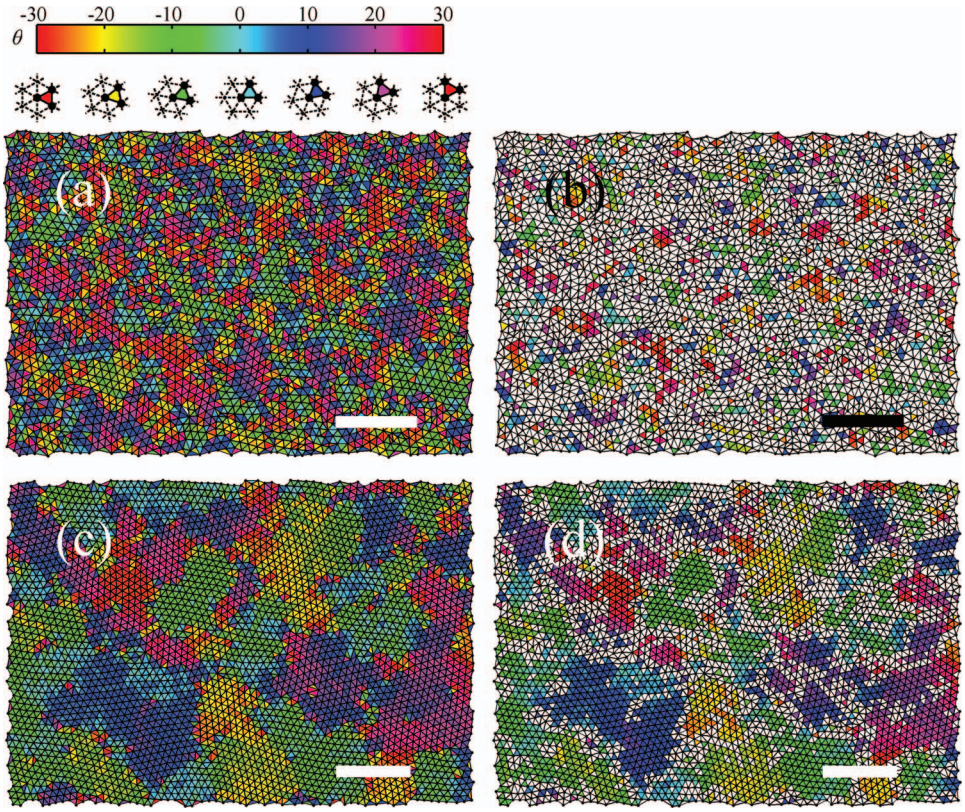

FIG. 3. Color-coded patterns with pore centers as triangle mesh nodes, and triangles are colored according to their orientation θ. (a, b) correspond to the pore structure in Figure 1(b); (c, d) correspond to Figure 1(f). Both Tol_d and Tol_ϕ are equal to 1 in (a, c), and 0.1 in (b, d).

than that in the top pattern. However, this does not change the ordering tendency on increasing acid concentration, which is clearly verified by the ADF shown in Figures 2(e) and 2(f). One can see that the peak position of the ADF for all patterns are located at around 60°, and the higher the peak intensity and the narrower the full-width at half-maximum (FWHM), the closer is the pattern to the perfect hexagonal case. From both the top patterns in Figure 2(e) and bottom patterns in Figure 2(f), the best ordered pattern is formed under 0.8 M, while the worst ordered pattern is formed under 0.3 M. The ordering tendency with acid concentration is first increasing and then decreasing. Although RDF and ADF are useful in indicating the ordering tendency, they are not sensitive enough to distinguish between two patterns with similar pore-center and angle distributions, e.g. two patterns formed under 0.6 and 0.8 M in Figure 2(f). The method involving the AOD in Section II B 3 is more useful in overcoming above difficulties.

For each SEM figure shown in Figure 1, its triangularly meshed pattern is color-coded according to the orientation θ obtained by equation (3), and those truncated pores at the boundaries of the SEM micrograph with centers falling outside the frame region are excluded. As an example, Figures 3(a)–3(d) show the color-coded patterns at different tolerance levels corresponding to the porous structures shown in Figures 1(b) and 1(f), respectively. In Figures 3(a) and 3(c), both the tolerance factors Tol_d and Tol_ϕ, as stated in Section II B 3, were set equal to 1, which means all the triangles in the mesh pattern are included. From these figures, ordered grains in the pattern are clearly distinguishable by their different colors due to their orientations. Sudden change of color happens across grain boundaries, or at single-site defects within a grain, and the grain sizes in Figure 3(a) are obviously smaller than those in Figure 3(c). In Figures 3(b) and 3(d), both Tol_d and Tol_ϕ were set at a much smaller value at 0.1, and by this a lot of the triangles much different from the equilateral triangle are excluded, and these are colored white in the figures. At such a

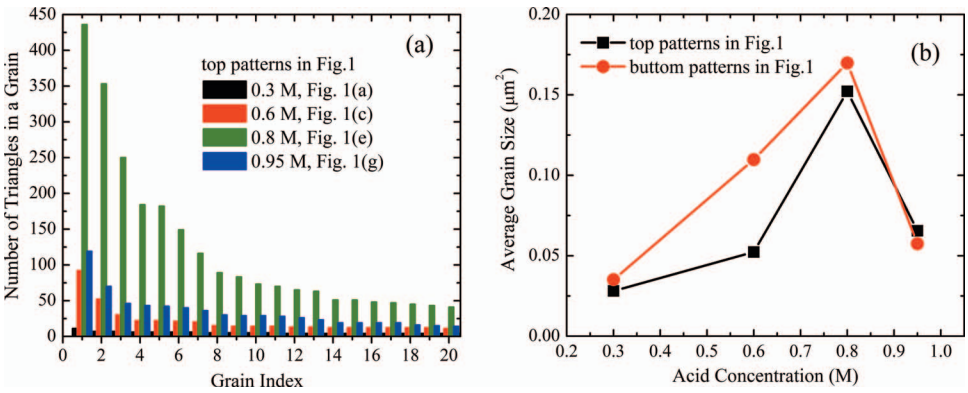

FIG. 4. (a) Number of triangles within the 20 largest grains in the patterns shown in Figures 1(a), 1(c), 1(e), and 1(g). (b) Average grain size against acid concentration for the patterns in Figure 1.

low acceptance level, the major part of the porous structure in Figure 3(b) is concluded amorphous (the white regions), whereas in the much better ordered structure in Figure 3(d), only those highly ordered regions are concluded as ordered grains which are colored.

Under above acceptance level of $Dev\_d < Tol\_d = 0.1$ and $Dev\_\phi < Tol\_\phi = 0.1$, which was chosen by referring Refs. 19 and 20, ordered grains (colored) are revealed and their sizes can be conveniently calculated. Even within one grain the orientation values θ of the triangles are not exactly the same, and so if the difference $\Delta\theta$ of two neighboring triangles is less than Tol_θ, these two triangles are accepted into the same grain. After checking many possible values in the range $[1^\circ, 10^\circ]$, Tol_θ was chosen to be 3°, since too small a value will divide up one grain into several tiny ones, while too large a value will combine two different grains together. It is worth noting here that some ambiguity does exist in defining where are the grain zones in a given pore pattern, especially when ordering is low. The demarcation of grains is controlled by the tolerance factors and the difficulty to unambiguously select these was discussed in Ref. 19. The choice of $Tol\_d = 0.1$, $Tol\_\phi = 0.1$ and $Tol\_\theta = 3^o$ here is judged to be appropriate after considering the effects of other values, and in order to be consistent, these tolerance values are used the same in the remaining of this paper. Figure 4(a) shows the number of triangles in each of the twenty largest grains in the patterns shown in Figures 1(a), 1(c), 1(e), and 1(g), respectively. It is clear that the pattern formed under 0.8 M has the largest grains than the other three patterns, and its largest grain consists of 436 triangles, and there were 92 grains in total (only the largest 20 are shown in Figure 4(a)). It is noted above in Figure 2(e) that the ADF fails to distinguish between the ordering under 0.6 M and 0.95 M acid concentration, but the angular orientation distribution (AOD) method in Figure 4(a) can reveal a noticeable difference: the blue histogram for the 0.95 M top pattern clearly exhibits better ordering than the red histogram for the 0.6 M top pattern. For a given porous pattern, it is desirable to have a single measure of the average grain size which could also be an indicator for the ordering, but evaluation of this quantity may be distorted if very small grains, such as those containing fewer than six triangles, are not excluded. In fact, regions containing fewer than six triangles are really merely describable as short-range ordered with at most only the nearest-neighbors identifiable, and hence they should not be qualified as ordered grains. For this reason, these regions with fewer than six triangles within are excluded in the average grain size calculation, and Figure 4(b) shows the average grain sizes of all of the patterns in Figure 1 plotted against the acid concentration. We noted above in Figures 2(b), 2(c), and 2(f) that the RDF and ADF cannot effectively distinguish between the ordering quality of the 0.6 M and 0.8 M bottom patterns, but in Figure 4(b), the AOD method clearly shows that the average grain size is significantly different at about 0.11 μm^2 and 0.17 μm^2 at 0.6 M and 0.8 M respectively. Figure 4(b) shows that the dependence of the ordering tendency of the porous structures on the acid concentration is more obvious than what can be revealed by the ADF and RDF in Figure 2. From Figure 4(b), the ordering first increases with acid concentration from 0.3 M to 0.8 M, and then decreases from 0.8 M to 0.95 M.

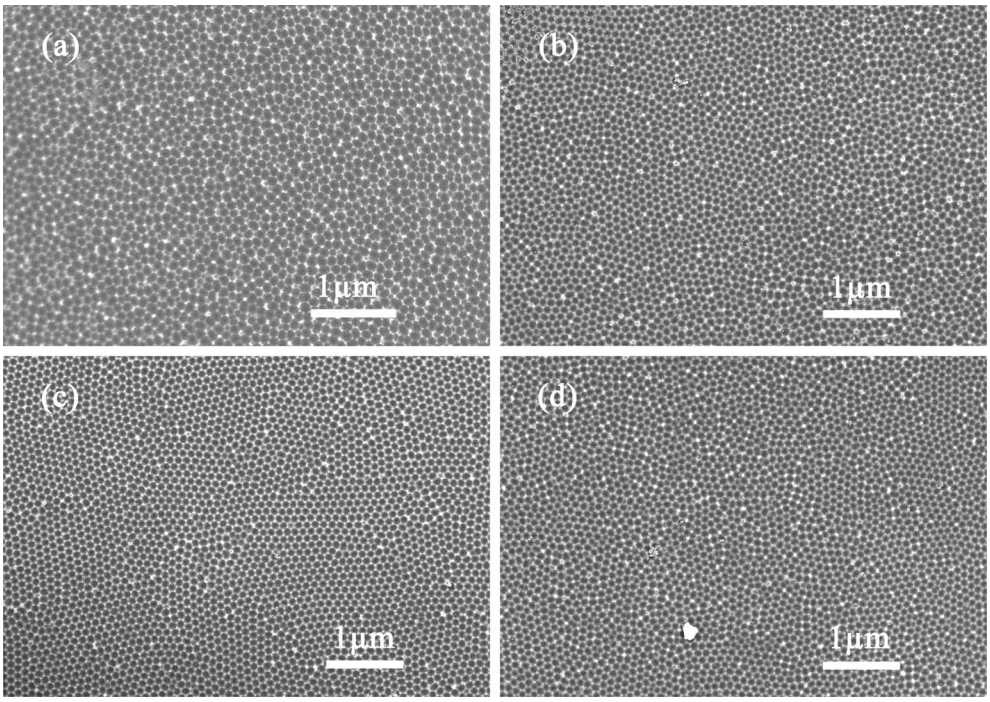

FIG. 5. SEM micrographs of bottom patterns on the aluminum substrate after selectively removing the anodic porous alumina on top. One-step anodization was conducted in (a) 0.05 M; (b) 0.3 M; (c) 0.4 M; (d) 0.45 M oxalic acid at 40 V at 2 °C for about 20 h.

The AOD results in Figure 4(b) also indicate that at the acid concentration of 0.6 M, ordering in the bottom pattern is better than that in the top pattern. This is in accordance with the sharper ADF of the bottom pattern (red curve in Figure 2(f)) than that in the top pattern (red curve in Figure 2(e)), as well as the higher first peak in the RDF of the bottom pattern than the top pattern in Figure 2(b). While an improvement of ordering as the oxide layer grows could be understood as a general trend, there is no particular reason to explain why this is more obvious for the 0.6 M concentration. The important point here, however, is that the three analysis methods of RDF, ADF, and AOD are consistent in this respect.

In order to investigate the effects of acid concentration at other temperatures, two groups of anodization experiments were done at 2 °C and 10 °C. As shown in Figures 5(a)–5(d), one-step anodization was conducted under acid concentrations of 0.05 M, 0.3 M, 0.4 M, and 0.45 M, respectively, at 40 V at 2 °C for about 20 h. Here, we focus on the pore bottom region revealed by the aluminum substrates after selectively removing the anodic oxide. From the RDF shown in Figures 6(a)–6(d), on increasing acid concentration the pattern's ordering quality first increases from 0.05 M to 0.4 M, and then decreases from 0.4 M to 0.45 M. This trend is similar to that at 20 °C shown in Figures 1 and 4(b), although the optimal acid concentration for the best ordering pattern is 0.4 M at 2 °C and 0.8 M at 20 °C. The trend noted from the RDF is also verified by the ADF as shown in Figure 6(e) – the ADF curve under 0.4 M has the narrowest FWHM.

Under the same tolerance conditions of Tol_d, Tol_ϕ, and Tol_θ as in Figure 4, the number of triangles in the first 20 largest grains and the average grain size in each pattern shown in Figure 5 are plotted in Figures 7(a) and 7(b), respectively. As shown in Figure 7(a), the number of triangles is very sensitive to the ordering quality the porous pattern. For example, if one compares the ordering quality between Figures 5(b) and 5(c) by direct observation, or by RDF in Figures 6(b) and 6(c), the difference is far less than what the red histogram at 0.3 M and the green histogram at 0.4 M in Figure 7(a) shows. The trend of the ordering tendency with acid concentration in both Figures 7(a) and 7(b) is the same as that shown by the ADF Figure 6(e), namely, the ordering increases first from 0.05 M to 0.4 M, and then decreases from 0.4 M to 0.45 M.

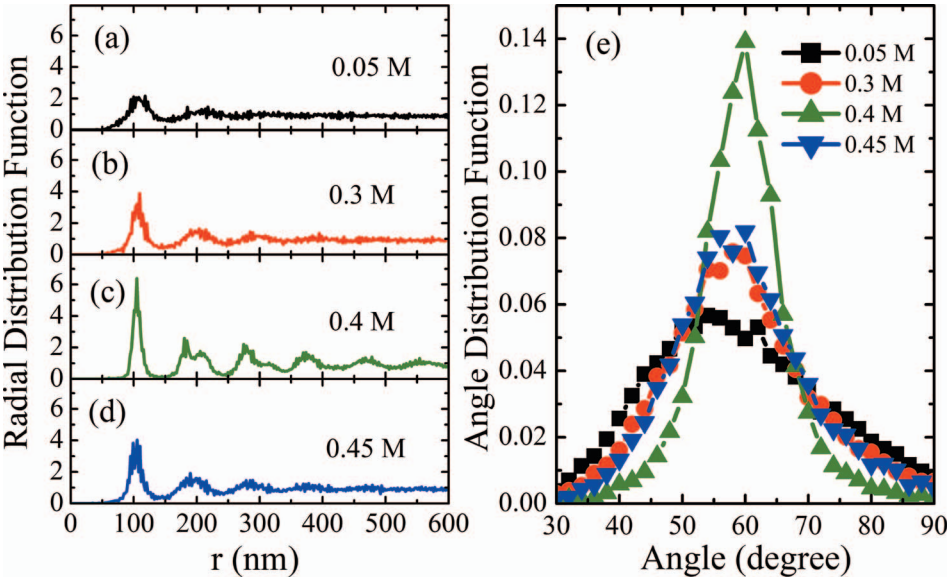

FIG. 6. (a-d) Radial distribution functions and (e) angle distribution functions for patterns shown in Figures 5(a)–5(d), respectively.

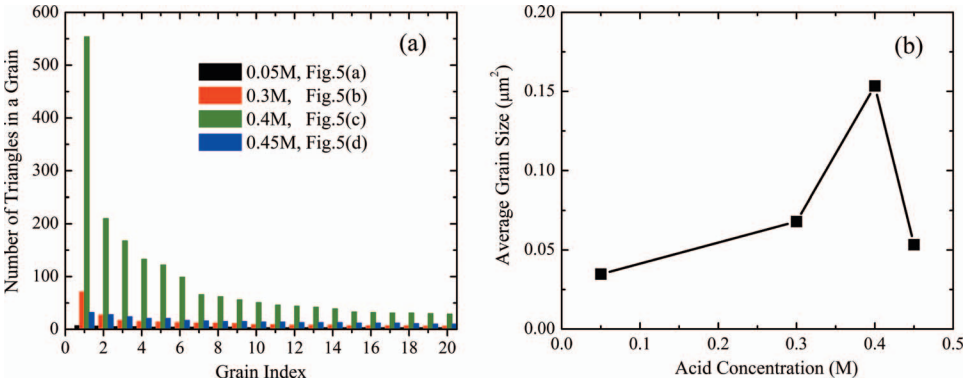

FIG. 7. (a) Number of mesh triangles in each of the 20 largest grains in the structures shown in Figure 5. (b) Average grain size of the patterns in Figure 5 against acid concentration.

Two-step anodization was conduction under 0.1 M, 0.3 M, and 0.6 M oxalic acid, respectively, under 10 °C for 2 h in the first step and a further 1 h in the second step. Figures 8(a)–8(c) show the bottom patterns on the aluminum substrate after selectively removing the anodic porous alumina. From Figure 8(d), one can easily see that the optimal acid concentration which gives rise to best ordering is 0.6 M.

It should be noted that the highest acid concentration used in the anodization at the three temperatures of 20 °C, 2 °C, and 10 °C in Figures 1, 5, and 8, namely, 0.95 M, 0.45 M, and 0.6 M respectively, is already close to the solubility limit of aqueous oxalic acid at each temperature. From the results in Figures 4, 7, and 8(d), we can conclude that the optimal oxalic acid concentration for the best ordering at 40 V is 0.8 M, 0.4 M, and 0.6 M at 20 °C, 2 °C, and 10 °C respectively. Together with the earlier established result that the optimal oxalic acid concentration is 0.3 M at 0 °C (Ref. 1), the relationship between the optimal acid concentration and temperature is plotted in Figure 9(a).

From Figure 9(a), the optimal oxalic acid concentration (square symbols) which can result in the best self-ordering in the pore arrangement is approximately linearly increasing with temperature. This means that at different temperatures, anodization in oxalic acid under 40 V would exhibit an optimal acid concentration corresponding to best ordering which is in general not 0.3 M. Moreover,

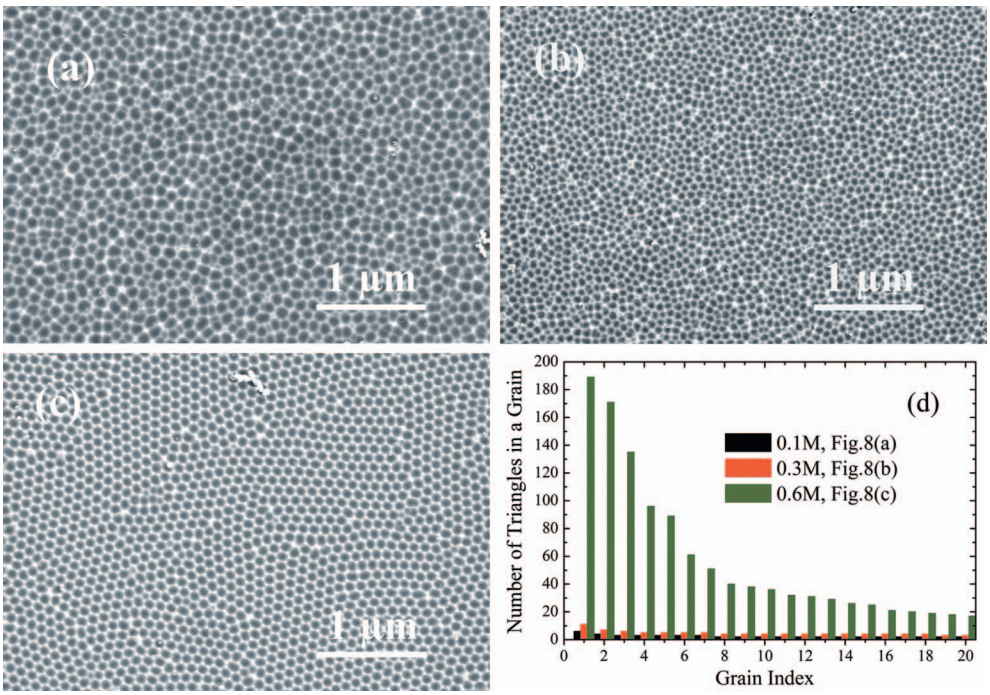

FIG. 8. (a-c) SEM micrographs of bottom patterns on the aluminum substrate after selectively removing the anodic porous alumina. Two-step anodization was conducted in (a) 0.1 M; (b) 0.3 M; (c) 0.6 M oxalic acid at 40 V at 10 °C for 2 h in the first step and 1 h in the second step. (d) Number of triangles in each of the 20 largest grains in the patterns of Figures 8(a)–8(c).

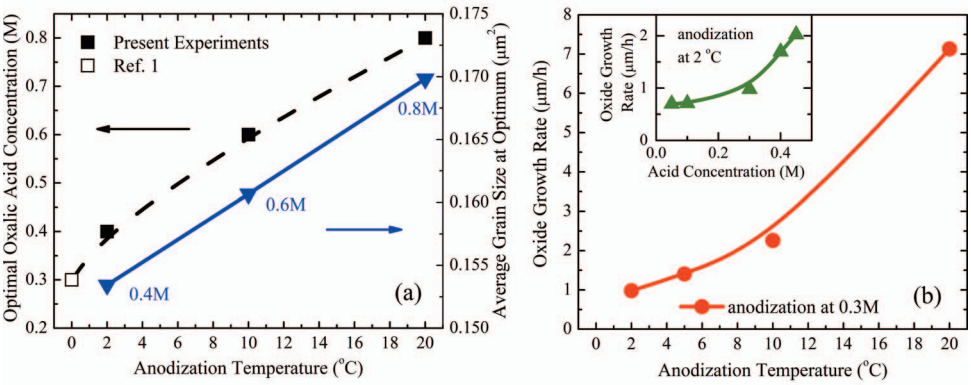

FIG. 9. (a) Optimal oxalic acid concentration (square symbols) which can result in the best pore-channel ordering in anodic porous alumina at 40 V, and average grain size (triangle symbols) formed under the optimal acid concentration, against anodization temperature; (b) Oxide growth rate against anodization temperature under 0.3 M oxalic acid at 40 V; the inset figure shows the oxide growth rate against oxalic acid concentration at 40 V at 2 °C.

under above optimal acid concentrations (0.4 M at 2 °C, 0.6 M at 10 °C, and 0.8 M at 20 °C), the average grain size (triangle symbols) is also slightly linearly increasing with temperature. In addition, one of the main limitations previously for the wide application of mild anodization is that the oxide growth rate is too slow for batch production.[2,17] However, this difficulty can be overcome if self-ordered porous alumina is fabricated using the optimal acid concentrations at higher temperatures as shown in Figure 9(a). Figure 9(b) shows that the oxide growth rate, estimated as the SEM observed oxide thickness divided by the anodization time, increases approximately exponentially with temperature under a certain acid concentration, and with acid concentration under a certain temperature. Therefore, on increasing temperature along the curve for optimal conditions in Figure 9(a), the oxide growth rate should increase enormously, since both temperature and acid concentration

are increasing, and both of them result in approximately exponentially increase of the oxide growth rate in Figure 9(b).

IV. CONCLUSIONS

Acid concentration and temperature dependent self-ordering conditions of anodic porous alumina formed by anodization of aluminum in oxalic acid under 40 V are quantitatively characterized. A novel method involving the angular orientation distribution of the triangles connecting three neighboring pore centers is found to be much more sensitive in delineating the ordering qualities than the radial distribution function and the angle distribution function. Quantitative analysis of the experimental results shows that under each temperature there exists an optimal oxalic acid concentration which leads to the best self-ordering porous pattern of anodic porous alumina. Both the optimal acid concentration and its resulted average grain size in the porous pattern increase approximately linearly with temperature. The oxide growth rate increases approximately exponentially with acid concentration and also with temperature. The results suggest that fast fabrication of self-ordered anodic porous alumina can be realized by performing the anodization at relatively higher temperatures using the corresponding optimal acid concentrations.

ACKNOWLEDGMENTS

C.C thanks Prof. N. R. Aluru for providing him a visiting scholar position at the University of Illinois at Urbana-Champaign. The authors thank S. Wang for help in fabricating the anodization setup used in this work. The work described in this paper was supported by grants from the Research Grants Council (Project No. HKU7159/10E), as well as from the University Grants Committee (Project No. SEG-HKU06) of the Hong Kong Special Administration Region, P.R. China.

[1] H. Masuda and K. Fukuda, Science **268**, 1466 (1995).
[2] W. Lee, R. Ji, U. Gösele, and K. Nielsch, Nature Mater. **5**, 741 (2006).
[3] K. Nielsch, J. Choi, K. Schwim, R. B. Wehrspohn, and U. Gösele, Nano Lett. **2**, 677 (2002).
[4] X. Y. Zhang, G. H. Wen, Y. F. Chan, R. K. Zheng, X. X. Zhang, and N. Wang, Appl. Phys. Lett. **83**, 3341 (2003).
[5] S. L. Sung, S. H. Tsai, S. H. Tseng, F. K. Chiang, X. W. Liu, and H. C. Shih, Appl. Phys. Lett. **74**, 197 (1999).
[6] W. Lee, H. Han, A. Lotnyk, M. A. Schubert, S. Senz, M. Alexe, D. Hesse, S. Baik, and U. Gösele, Nature Nanotechnology **3**, 402 (2008).
[7] H. Masuda, M. Yamada, F. Matsumoto, S. Yokoyama, S. Mashiko, M. Nakao, and K. Nishio, Adv. Mater. **18**, 213 (2006).
[8] A. L. Friedman and L. Menon, J. Appl. Phys. **101**, 084310 (2007).
[9] H. Asoh, K. Nishio, M. Nakao, T. Tamamura, and H. Masuda, J. Electrochem. Soc. **148**, B152 (2001).
[10] F. Li, L. Zhang, and R. M. Metzger, Chem. Mater. **10**, 2470 (1998).
[11] H. Masuda, H. Yamada, M. Satoh, and H. Asoh, Appl. Phys. Lett. **71**, 2770 (1997).
[12] H. Masuda, M. Yotsuya, M. Asano, K. Nishio, M. Nakao, A. Yokoo, and T. Tamamura, Appl. Phys. Lett. **78**, 826 (2001).
[13] H. Masuda, A. Abe, M. Nakao, A. Yokoo, T. Tamamura, and K. Nishio, Adv. Mater. **15**, 161 (2003).
[14] A. S. M. Chong, L. K. Tan, J. Deng, and H. Gao, Adv. Funct. Mater. **17**, 1629 (2007).
[15] S. Z. Chu, K. Wada, S. Inoue, M. Isogai, and A. Yasumori, Adv. Mater. **17**, 2115 (2005).
[16] K. H. Lee and C. C. Wong, J. Appl. Phys. **106**, 104305 (2009).
[17] D. Losic, M. Lillo, and D. Losic Jr. Small **5**, 1392 (2009).
[18] W. Lee, J. C. Kim, and U. Gösele, Adv. Funct. Mater. **20**, 21 (2010).
[19] R. Hillebrand, F. Müller, K. Schwirn, W. Lee, and M. Steinhart, ACS Nano **2**, 913 (2008).
[20] S. Mátéfi-Tempfli, M. Mátéfi-Tempfli, and L. Piraux, Thin Solid Films **516**, 3735 (2008).
[21] A. C. Galca, E. S. Kooij, H. Wormeester, C. Salam, V. Leca, J. H. Rector, and B. Poelsema, J. Appl. Phys. **94**, 4296 (2003).
[22] K. Y. Ng, Ph. D. thesis, The University of Hong Kong, 2009.
[23] ImageJ, a software designed by W. Rasband, version 1.44p, NIH: USA, public domain, http://rsb.info.nih.gov/ij/.